UDC 544.463:[546.72+546.824:546.261]

Mechanochemcial Synthesis of Nanocomposites from Different Precursors in Fe–Ti–C System

S. F. LOMAEVA, I. V. POVSTUGAR, V. A. VOLKOV, A. N. MARATKANOVA and E. P. YELSUKOV

Physical-Technical Institute, Ural Branch of the Russian Academy of Sciences, Ul. Kirova 132, Izhevsk 426000 (Russia)

E-mail: uds@pti.udm.ru

Abstract

X-ray diffraction, Mössbauer and Auger electron spectroscopy, electron and atomic force microscopy were employed in order to study the sequence of structural phase transformations in the course of mechanical alloying (MA) and annealing the iron–titanium–carbon system obtained from the mixtures of different compositions: powders of pure elements Fe (70 at. %), Ti (15 at. %), graphite (15 at. %); Fe (70 at. %) and TiC (30 at. %) powders; Fe (70 at. %) and Ti (15 at. %) powders with toluene. It has been demonstrated that in all the cases the MA results in the formation of nanocomposite powders with a complicated phase composition such as solid solution based on Fe, roentgen-amorphous phase based on carbides TiC and Fe_3C, carbide TiC. Annealing results in the crystallization of the amorphous phase, decomposition of the solid solution and formation of nanocomposite Fe + TiC + Fe_3C. The dispersity, number and the composition of carbide phases depend on MA conditions. In the case of Fe, Ti and toluene mixture, by varying MA time one can obtain a two-phase Fe + TiC system with the uniform distribution of nanocrystalline phases in the sample.

Key words: mechanical alloying, nanocomposites, titanium carbide, cementite

INTRODUCTION

Among composite materials based on metals, an extensive application in the industry is found by hard alloys and carbide-steel those represent composites with a carbide reinforcing phase regularly distributed within viscous metal matrix. The level of plasticity, durability, hardness and wear resistance of such composites is determined both by physicomechanical properties of a metal coupler and carbide reinforcing phase, and by their structure [1, 2]. The most important characteristics of the structure are presented by dispersity and a volumetric content of the carbide phase. It is commonly known that due to a high dispersity (less than 100 nm) of phases and crystallites in nanostructurized materials one could realize an additional possibility for improving useful properties [3–5]. From this point of view, obtaining and studying the nanostructurized analogues of hard alloys and carbide-steel, obtained via the method of mechanical alloying (MA) is of a considerable interest.

Due to a unique complex of properties (high hardness, thermal and chemical stability, temperature conductivity, low density), titanium carbide TiC is a prospective material for application as a reinforcing phase in high-strength and hard alloys as a material for machining tools and as a basis foe ceramic materials and metal-ceramic composites. Usually Fe–TiC composites are obtained using high-temperature methods [1, 2, 6], which is connected with a required use of heat-resistant materials as well as with a high energy consumption in the course of synthesis.

In this connection is of interest to study the possibility of synthesizing such composites in nanocrystalline state in the process of MA. On the other hand, the technology for preparing carbide steel includes the use of organic liquids (gasoline, acetone, ethyl alcohol, cyclohexane) as an environment for grinding [1, 2], however the influence of an organic environment for grinding upon the process of forming the structure, phase composition and properties of the alloys under obtaining is not investigated up till now.

The purpose of the present work consists in the studies on the sequence of structure - phase transformations in the iron–titanium–carbon system under different MA conditions and subsequent annealing.

EXPERIMENTAL

Mechanical alloying (MA) procedure was carried *via* three methods using the mixtures with the following composition:

1) Powders of iron, titanium, graphite at a ratio 70 : 15 : 15 at. %, in the environment of argon, the duration of MA (t_{MA}) amounted to 1, 2, 4, 8, 16 h (sample Fe–Ti–C);

2) Powders of iron and titanium carbide TiC at a ratio 70 : 30 at. %, in the environment of argon, t_{MA} = 1, 2, 4, 8, 16 h (sample Fe–TiC);

3) Powders of iron and titanium at a ratio 70 : 15 at. %, in the environment of toluene, t_{MA} = 16, 20, 32 h (sample Fe–Ti–toluene).

The mechanical alloying was carried out in a Fritsch P-7 planetary ball mill (Germany) with the acceleration of 25*g*. Mill vessels 45 cm^3 in volume and milling balls (20 balls, 10 mm in diameter) were made of ShKh15 steel (1 % C and 1.5 % Cr) with high hardness and a minimal content of alloying elements in order to minimize the contamination of powders by extraneous impurities. With the use of forced air cooling, the warming of the external wall of vessels during the mill operation did not exceed 80 °C.

Samples were annealed under vacuum of 10^{-3} Pa at the temperature values amounting to 500, 600, 700, 800 °C, during 1 h.

X-ray diffraction structural studies were carried out employing DRON-3M diffractometer with filtered CuK_α radiation. Qualitative and quantitative X-ray diffraction phase analysis, as well as determining the parameters of crystal lattice were carried out with the use of a software package presented in [7, 8].

Mössbauer spectra were obtained using YaGRS-4M spectrometer in a constant acceleration mode with ^{57}Co(Cr) source. In order to calculate the distribution of superfine magnetic field $P(H)$ we used the method of regularization [9].

Auger electron spectra were obtained using JAMP-10S spectrometer at the accelerating voltage amounting to 10 kV, current strength 10^{-7} A, electron probe diameter equal to 300 nm; electron microscopy images were obtained with the use of secondary electrons. The vacuum level in the spectrometer chamber amounted to 10^{-7} Pa. The etching of samples was performed using Ar ions with 3 keV energy; the etching rate reached approximately 0.3 nm/min. The analysis of spectra was carried out employing a technique described in [10].

The atomic force microscopy (AFM) studies were performed using P47-SPM-MDT scanning probe microscope in air, in a semi-contact mode (tapping mode) for powders after annealing at 500 °C. Silicon cantilevers were used. The probe represented a cone with the convergence angle at the top less than 20°, 7 μm high and with the needle curvature radius less than 10 nm. In order to reveal phase structural features, the surface was etched with 3 % nitric acid solution in ethyl alcohol [11]. After such a processing, ferrite only was etched, whereas carbides remained intact being well displayes in three-dimensional pictures of surface topography.

Metallographic studies were carried out for thin sections of powders mixed with epoxide resin, employing Neophot-2 microscope (Russia) with digital registration.

All measurements were performed at a room temperature.

RESULTS AND DISCUSSION

From the data presented in Fig. 1 one can see that after the MA the particles of Fe–Ti–toluene powder are of stone-like shape with the particle size ranging within 5–30 μm and homogeneous morphological structure. The particles of Fe–Ti–C and Fe–TiC powders are more gross, rounded consisting of a dark nucleus and a light shell; small fraction of particles is inherent in the presence of a light shell only (see Fig. 1, *c*, *d*).

Fe–Ti–C sample

Figure 2, *a* demonstrates X-ray diffraction patterns for samples after MA procedure performed during different exposition time. One can see that after 1 h of processing the diffraction pattern exhibits only reflexes corre-

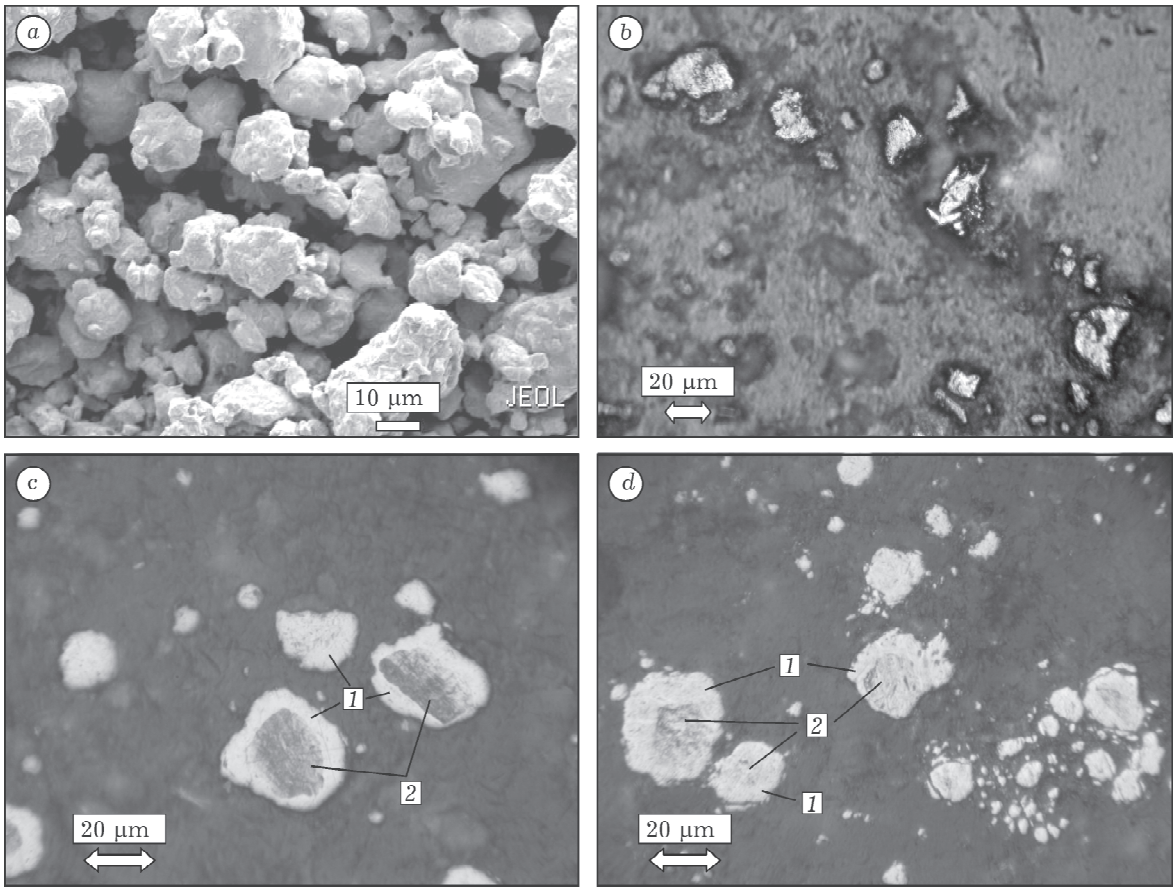

Fig. 1. Electron microscopy (*a*) and metallographic (*b*–*d*) images of powders after mechanical alloying procedure: *a*, *b* – Fe–Ti–toluene, t_{MA} = 20 h; *c* – Fe–Ti–C, t_{MA} = 16 h; *d* – Fe–TiC, t_{MA} = 16 h; *1* – shell, *2* – nucleus.

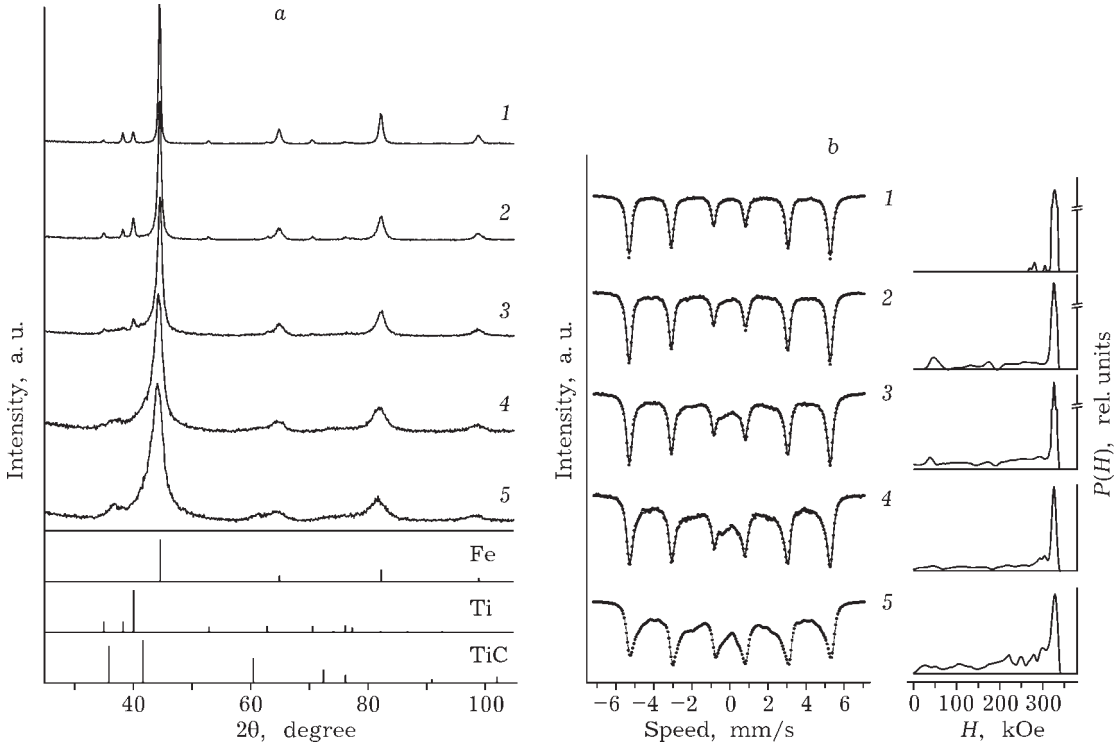

Fig. 2. XRD patterns (*a*) and Mössbauer spectra as well as distribution functions *P*(*H*) (*b*) for Fe–Ti–C sample after mechanical alloying procedure. Processing time, h: 1 (*1*), 2 (*2*), 4 (*3*), 8 (*4*), 16 (*5*).

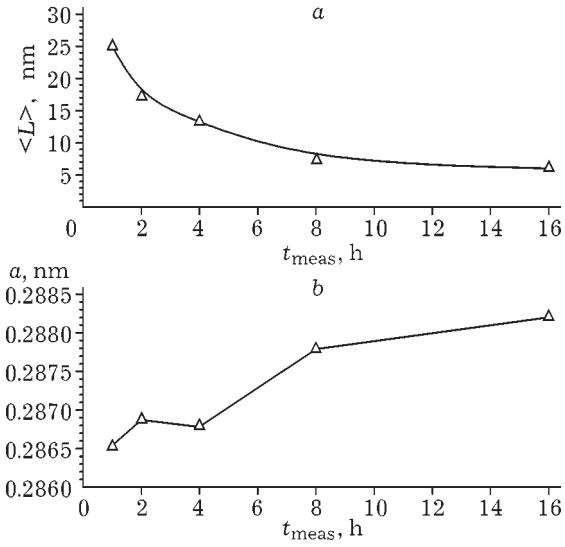

Fig. 3. Results of quantitative analysis for Fe–Ti–C sample after mechanical alloying. Grain size (*a*) and lattice parameter (*b*) for BCC phase on the basis of Fe.

sponding to α-Fe and α-Ti. The absence of graphite reflexes indicates a low atomic X-ray scattering factor, as well as carbon diffusion across metal grain boundaries, according to data of [12]. The broadening of the reflexes with an increase in MA procedure duration could be caused by decreasing the size of grains and increasing the level of microdeformations. After 4 h of MA procedure the intensity of reflexes for initial metals abruptly decreases, whereas the grain size of α-Fe decreases down to 13 nm (Fig. 3, *a*).

At the same time an increase of the background level is observed within a wide range of angles amounting to 35–55° and 65–90° (see Fig. 2, *a)* those are corresponding to the most intense reflexes of cementite Fe_3C and cubic titanium carbide TiC is observed. The latter could be interpreted as the formation of roentgen-amorphous phases based on carbides such as Fe_3C and TiC. With the further increase in MA procedure duration up to 8 and 16 h, against the background of amorphous halo there are considerably broadened TiC and Fe_3C reflexes. The grain size for both α-Fe and carbides amounts to 5–7 nm (Table 1). The results of phase analysis for the sample obtained at t_{MA} = 16 h, are presented in Table 2.

When the phase composition is calculated for atomic percentage (with the assumption that the structure of carbides is stoichiometric), only about 10 at. % of Ti bound in the TiC phase. Despite of high TiC formation enthalpy (−209 kJ/mol) [13], the MA process in Fe–Ti–C mixture results in a slow synthesizing of titanium carbide. In order to explain this fact the authors of [14, 15] proposed a mechanism for interdiffusion of components.

The lines of titanium carbide TiC are shifted towards greater 2θ angle values in comparison with the reference data [16]. This fact could be connected with non-stoichiometric composition of monocarbide (carbon deficiency therein), since titanium carbide TiC exhibits a wide concentration range of the existence [16], as well as with doping TiC with iron atoms. Another feature of the diffraction patterns consists in shifting α-Fe reflexes towards lower angle values, which reflects an increase in the lattice parameter (see Figs. 2, *a* and 3, *b)*.

This phenomenon, most likely, could be caused by a partial dissolution of titanium and, probably, carbon in the BCC of iron. If it is assumed that only titanium could be dissolved in α-Fe, the titanium content in α-Fe, according to [17], would be equal to 6 at. %. Taking

TABLE 1

Lattice parameter *a* and grain size <*L*> after mechanical alloying procedure (t_{MA} = 16 h) and annealing

Samples	Parameters	α-Fe			TiC*		
		MA	500 °C	800 °C	MA	500 °C	800 °C
Fe–Ti–C	*a*, ±0.0005 nm	0.2882	0.2869	0.2869			0.4256
	<*L*>, ±1 nm	6	10	25	<5	5	10
Fe–TiC	*a*, ±0.0005 nm	0.2873	0.2868	0.2869	0.4296	0.4288	0.4293
	<*L*>, ±1 nm	11	15	40	9	9	15
Fe–Ti–toluene	*a*, ±0.0005 nm	0.2878	0.2869	0.2868	0.4277	0.4274	0.4305
	<*L*>, ±1 nm	6	13	22	5	6	12

**Lattice parameter for TiC after MA and annealing at 500 °C was not determined due to a large-scale broadening and overlapping of lines.

TABLE 2

Phase composition of samples, mass % (±3 %)

Samples	t_{MA}, h	T_{ann}, °C	Fe	TiC	Fe_3C
Fe–Ti–C	16	Initial	56	16	28
		500	47	15	38
		800	45	17	38
Fe–TiC	16	Initial	78	22	0
		500	69	23	8
		800	69	23	8
Fe–Ti–toluene	16	Initial	77	23	0
		500	74	26	0
	20	500	57	25	18
		800	55	26	19
	32	500	27	20	53

into account that about 10 at. % of Ti is bound in TiC, the value obtained can be considered as that close to the initial content of Ti (15 at. %).

Figure 2, *b* demonstrates Mössbauer spectra for various stages of MA. At the initial stage, the spectra under consideration represent Fe sextet with insignificantly deformed lines, whereas with the increase in MA procedure duration a peak is observed to appear with $H = 300$ kOe (see Fig. 2, curves *4* and *5*), which confirms that there is dissolution Ti in α-Fe occurring.

After 2 h of MA exposed one can observe the deviation of the spectrum with respect to a non-resonant level, as well as the presence of a weak non-split component at the center of the spectrum. The distribution functions for superfine magnetic fields $P(H)$ reduced from the spectra indicate that there is a wide and rather flat distribution over the field intensity within the range of 0–300 kOe, whose contribution with respect to 16 h MA corresponding value amounts up to 50 %. This fact confirms the conclusion drawn from XRD data that the formation of the amorphous phase occurs on the basis Fe–C carbides. Insignificant amount of a non-split component could be attributed to the atoms of iron dissolved in carbide TiC.

Figure 4 demonstrates the results of XRD and Mössbauer analyses performed for Fe–Ti–C composite ($t_{MA} = 16$ h) after MA and annealing. The annealing at 500 °C results in the crystallization of the amorphous phase and the decomposition of the BCC solid solution on the basis of iron: the lattice parameter approximates to the standard value (see Fig. 3, *b* and Table 1), as well as to the disappearance of microdeformations in the BCC phase. The grain size for iron and carbides almost does not change (see Fig. 3, *a*).

The Mössbauer spectra of the powder at the annealing temperature $T_{ann} = 500$ °C exhibit a second sextet whose value $H = 208$ kOe obtained is in a good agreement with the data published earlier for carbide Fe_3C [18–20]. At $T_{ann} > 600$ °C, complete crystallization is observed for the amorphous phase to result in the formation of TiC, Fe_3C and α-Fe, which is displayed well on the diffraction patterns. The parameter of α-Fe lattice does not change with the increase in the annealing temperature. The Mössbauer spectra exhibit only two components remained corresponding to Fe and Fe_3C.

After annealing at 800 °C the size of Fe grains grows up to 25 nm, and that of titanium carbide and cementite increases up to 10 nm. Thus, the nanocrystalline state remains intact after annealing. The annealing does not result in a considerable changing in the phase composition of a sample. So, the amount of TiC remains previous, the amount of cementite (see Table 2) increases a little at the expense of carbon which was present as a solid solution in α-Fe and in the segregations on the boundaries of nanocrystallites [12].

The data of metallographic analysis indicate that there is non-uniform internal structure of the particles of Fe–Ti–C powder (see Fig. 1, *c*). The particles of coarse fraction powder are non-uniform and consist of a central (more dark) nucleus and a light shell. The majority of fine particles look so light. As it follows from the results of the Auger analysis of these areas (Fig. 5, *a* and Table 3), the nuclei of particles are enriched with titanium, whereas the shells are enriched with iron.

From AFM data (see Fig. 5, *b)* one can see that on the light sites the carbide particles formed under annealing those are manifested after etching as brighter inclusions, are in a uniform manner distributed in the sample. This fact indicates that there is a high level of uniformity of the components of the mixture within these areas. It is obvious that nuclei are formed at early stages of MA on the basis of particles of the powder with high titanium con-

tent . Such particles exhibit a greater hardness and are longer intact, therefore in the process of MA, a layer of softer products of the latest alloying stages is formed thereon. From this it follows that under the chosen conditions the MA duration amounting to 16 h it is not enough in order to obtain homogeneous distribution of components in the composite on the basis of the initial mixture of elementary Fe, Ti and graphite powders.

Basing on the results obtained one could propose the following scheme of the MA process resulting from elementary mixtures of powders. Under the action of plastic deformations the components are mechanically mixed with the simultaneous accumulation of defects and the reduction of grain size [21]. After the moment when nanocrystalline state is reached, at the boundaries of grains there begins an intense mutual diffusion of components to occur, which in combination with plastic deformation results in the formation of a solid solution and an amorphous phase [22–24].

The coefficient of grain-boundary carbon diffusion in nanocrystalline metal is very high [25], therefore the saturation of particles with carbon and the formation of cementite within iron particles and of titanium carbide within

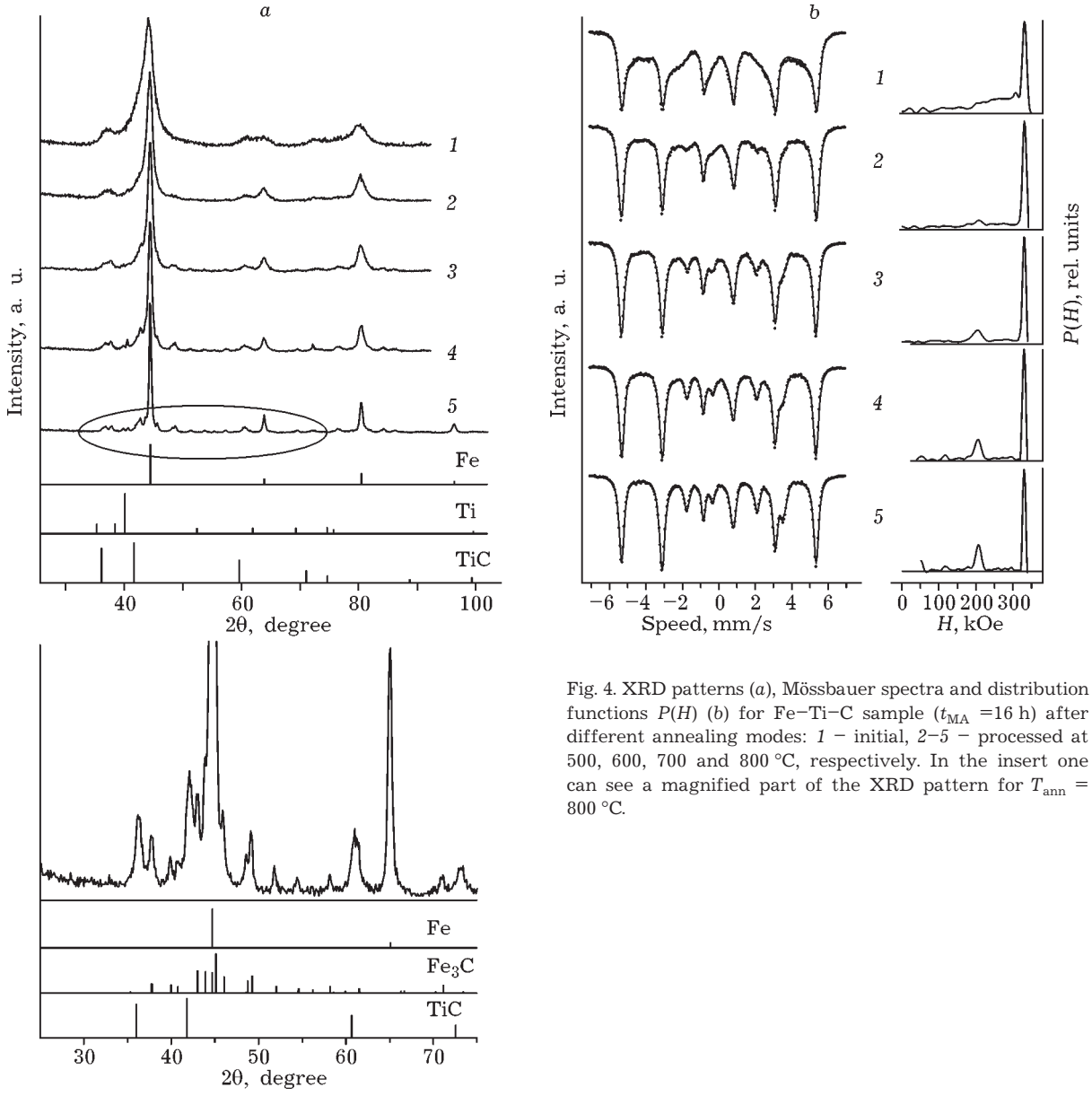

Fig. 4. XRD patterns (*a*), Mössbauer spectra and distribution functions $P(H)$ (*b*) for Fe–Ti–C sample (t_{MA} =16 h) after different annealing modes: *1* – initial, *2–5* – processed at 500, 600, 700 and 800 °C, respectively. In the insert one can see a magnified part of the XRD pattern for T_{ann} = 800 °C.

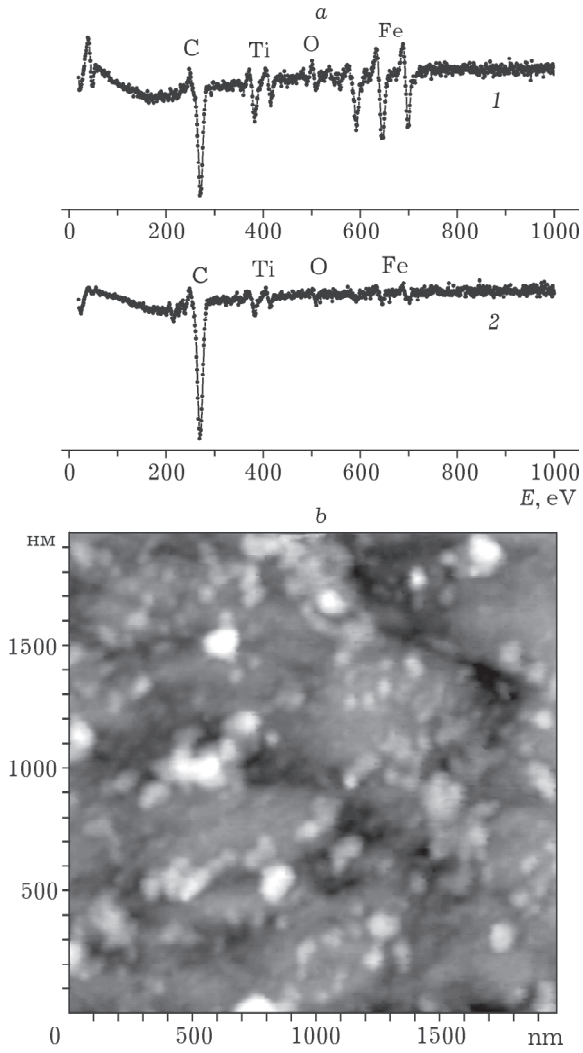

Fig. 5. Auger electron spectra of a shell (*1*) and nucleus (*2*) for coarse particles of Fe–Ti–C sample (*a*) and AFM image of the shell after ferrite etching (*b*).

TABLE 3

Results of Auger electron analysis of the composition Fe–Ti–C and Fe–TiC sample surface after annealing (T_{ann} = 500 °C), ±3 at. %

Samples	Area*	Fe	Ti	C	O	Fe : Ti
Fe–Ti–C	1	20	5	68	7	80 : 20
	2	6	3	87	4	65 : 35
Fe–TiC	1	15	7	66	12	70 : 30
	2	3	3	90	4	50 : 50

*Area 1 corresponds to a light shell of a particle, area 2 corresponds to a dark inclusion (nucleus) (see Figs. 1, *c*, *d* and 7).

titanium particles proceeds faster than the formation of Fe–Ti alloy. Further a joint plastic deformation of iron-cementite and titanium-carbide particles occurs. The light areas prevailing on the image are formed by particles based on iron, and dark areas are formed by particles formed on the basis of titanium.

Fe–TiC sample

Figure 6 demonstrates the results of XRD and Mössbauer analysis of the sample obtained *via* MA (t_{MA} = 16 h) with the mixtures of iron and titanium carbide TiC powders. As opposed to Fe–Ti–C sample, there is almost no amor-

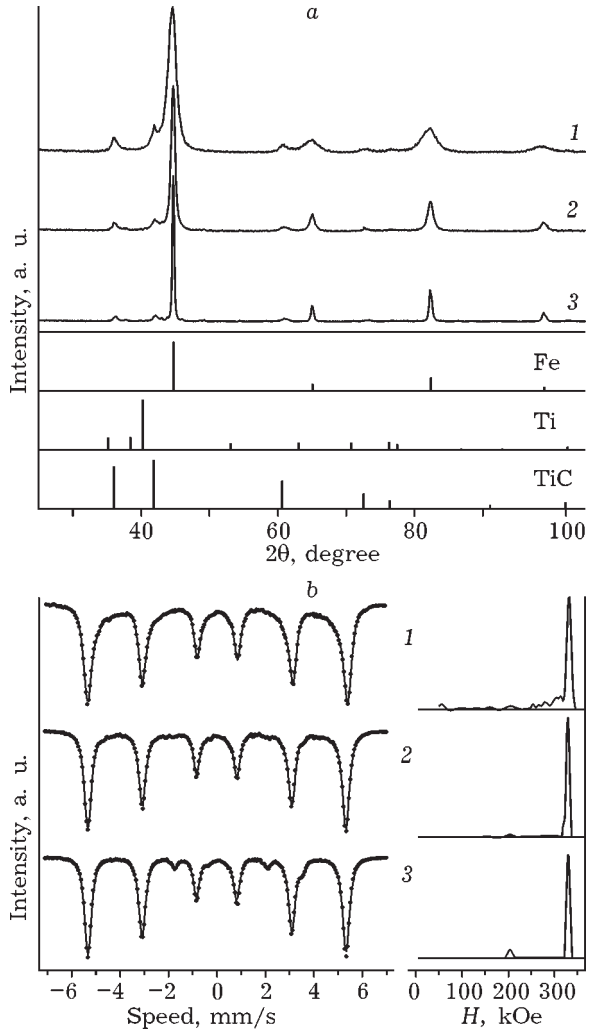

Fig. 6. XRD patterns (*a*), Mössbauer spectra and distribution functions $P(H)$ (*b*) for Fe–TiC sample: *1* – after mechanical alloying procedure during 16 h; *2*, *3* – annealed at 500 and 800 °C, respectively.

phous phase in this sample after MA procedure. The lines of carbide TiC are not shifted comparing to the reference, *i.e.* the structure of carbide does not change in the process of MA. There is a small increase in the parameter of Fe lattice observed (up to 0.2873 nm), which indicates that the dissolution of the titanium in iron occurs. However, for Fe–TiC sample the amount of titanium dissolved in iron is less comparing to Fe–Ti–C (≈3 at. %) (see Table 1). The grain size of Fe and TiC amounts to 11 nm. The Mössbauer spectral data indicate the occurrence of titanium in iron, too: a distortion of the lines disappearing after annealing is observed.

After annealing at 500 °C the parameter of iron lattice approaches to the reference value, the size of grains for iron titanium carbide almost does not change. After annealing at 800 °C the size of iron grain amounts to 40 nm, the grain size for titanium carbide amounts up to 15 nm. The X-ray diffraction patterns and Mössbauer spectra exhibit Fe_3C phase (about 8 mass %, see Table 2). The formation of Fe_3C, to all appearance, could be caused by the presence of free carbon in the initial carbide and by the dissolution of titanium carbide in the course of MA processing. The content of TiC phase after annealing amounts to 23 at. %, which is less than the content in the initial sample (30 at. %).

Figure 1, *d* demonstrates the microstructure of Fe–TiC powder particles after MA procedure during 16 h. Just as in the case of Fe–Ti–C powder, the particles of coarse fraction consist of a nucleus and a shell. The distinctive feature of the microstructure of Fe–TiC powder consists in the presence of dispersed inclusions of TiC remained intact as a result of grinding of the initial powder. The nuclei contain much more such inclusions in comparison with the shell of particles. In this case, more hard particles of powder consisting mainly of TiC inclusions, are inherent in the formation thereon of the products resulted from later MA stages.

The Auger spectra obtained for metal matrix and carbide inclusions of Fe–TiC powder are demonstrated in Fig. 7, *a*, the quantitative analysis data are presented in Table 3. The results confirm that the inclusions represent the particles of non-dissolved titanium carbide. The surface of a carbide particle is covered by car-

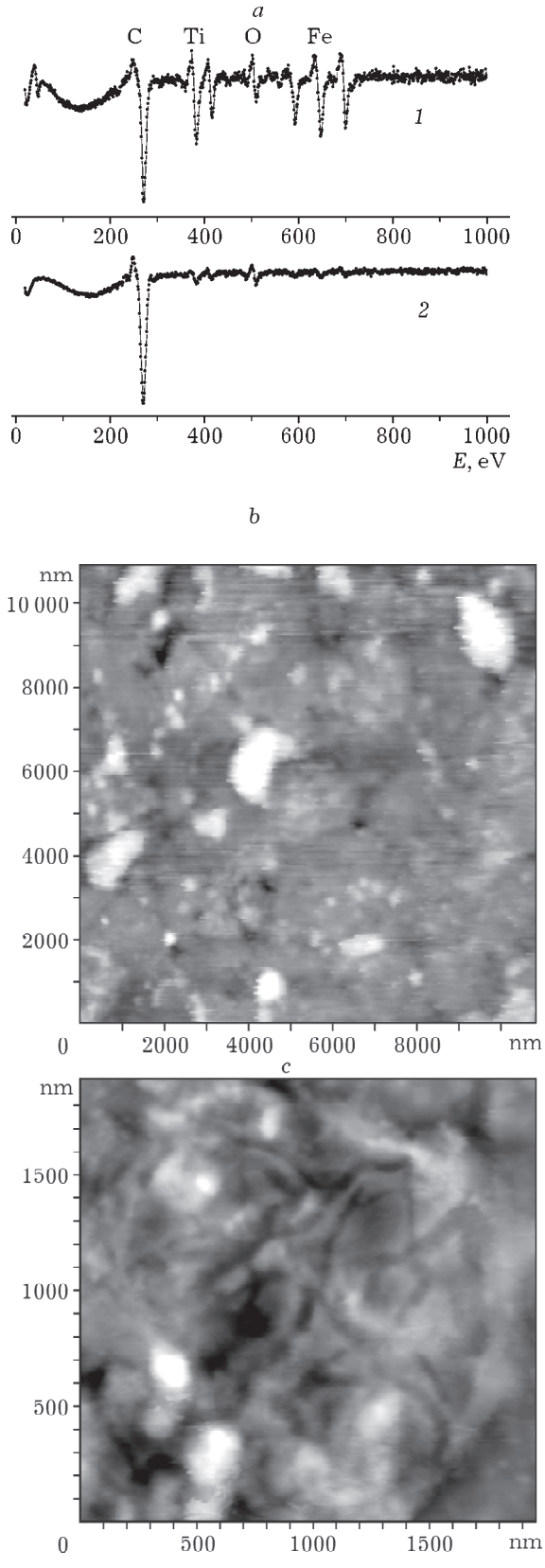

Fig. 7. Auger electron spectra for a metal matrix (*1*) and inclusions (*2*) in Fe–TiC powder (*a*) and AFM image for a metal matrix (*b*) and nucleus (*c*).

bon, which is exhibited by an increased intensity of carbon lines and lowered intensity of lines corresponding to other elements in Auger spectrum. In the same manner as for Fe–Ti–C sample, titanium is present in the structure of iron matrix, and iron is present in the structure of inclusions based on titanium carbide.

From AFM data for the etched surface of powder particles' section (see Fig. 7, *b*) one can see that besides homogeneously distributed fine secondary carbide particles with the grain size up to 100 nm, there are considerably more coarse (1–10 μm) non-dissolved titanium carbide particles. On the AFM image of a large carbide inclusion (see Fig. 7, *b*) one can see well a layered structure, *i.e.* the MA process within large carbide particles occurs at an initial stage such as the stage of forming a curtailed layered structure [26].

Thus, the results obtained allow us to propose the following scheme of the MA process for Fe–TiC system. Under the action of intense plastic deformations, the formation of nanocrystalline structure in iron, grinding of fragile titanium carbide as well as the dissolution of fine titanium carbide particles in iron according to the mechanism suggested in work [27]

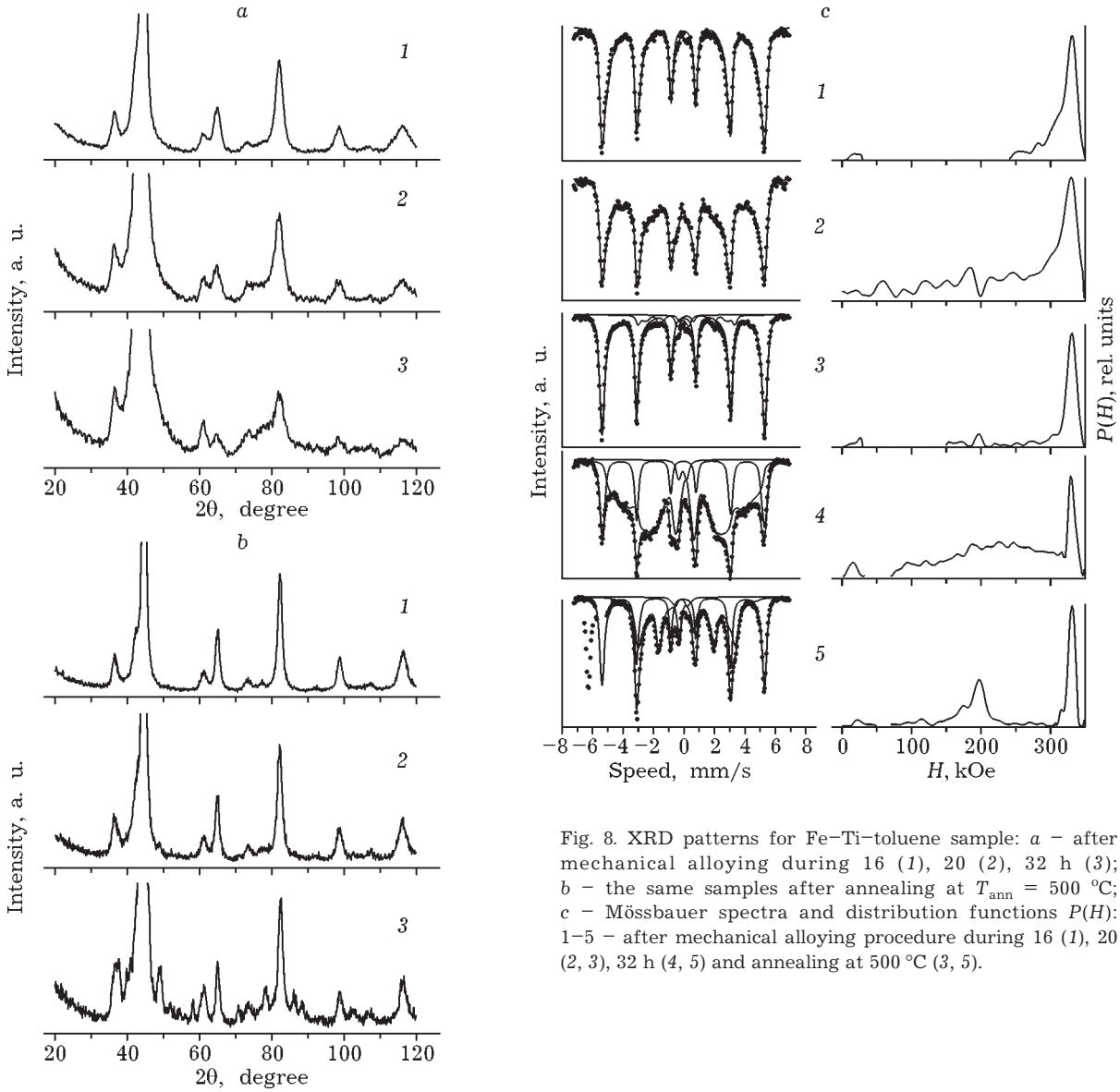

Fig. 8. XRD patterns for Fe–Ti–toluene sample: *a* – after mechanical alloying during 16 (*1*), 20 (*2*), 32 h (*3*); *b* – the same samples after annealing at T_{ann} = 500 °C; *c* – Mössbauer spectra and distribution functions *P*(*H*): 1–5 – after mechanical alloying procedure during 16 (*1*), 20 (*2*, *3*), 32 h (*4*, *5*) and annealing at 500 °C (*3*, *5*).

are observed to occur. In addition there is the formation of Ti and C solid solution in iron and then the formation of the secondary Fe_3C and TiC carbides within the particles of iron. Since the inclusions of titanium carbide partly remain coarse, one could assume that in the case of a Fe–TiC sample the duration of MA procedure (16 h) appeared not enough in order to obtain a homogeneous distribution of nanocrystalline phases within a sample.

Fe–Ti–toluene sample

It has been established that under MA the behaviour of a Fe–Ti–toluene sample is in many respects similar to the behaviour of Fe–Ti–C sample. Figure 8 demonstrates the results of XRD and M**o??**ssbauer analyses of the sample. After the MA procedure, the lines of titanium carbide TiC are shifted towards higher values of 2θ angle in comparison with data of [16], which indicates that there is TiC doping with iron atoms observed. This fact is also confirmed by the fact that presence a component within the magnetic field range of 0–50 kOe is present in the $P(H)$ function. The reflexes of α-Fe are shifted towards lowere angles, which reflects an increase in the lattice parameter (0.2878 nm) due to Ti dissolution in Fe (≈5 at. %) being also confirmed by the presence a peak with H = 300 kOe in the $P(H)$ functions (see Fig. 8, *c*, curves *1*, *2*, *4*). The grain size of iron and titanium carbide amounts to about 6 nm (see Table 1).

The main difference consists in the fact that the MA process results first of all in the formation formed of titanium carbide, and only when almost all the titanium turns into carbide, there starts the formation of cementite whose amount grows with the increase in MA duration time (see Table 2). After annealing, the destruction of solid solution occurs, the lattice parameter value approaches to the initial one (0.2868 nm). After annealing at the temperature of 800 °C the grain size of α-Fe increases up to 22 nm, the grain size of titanium carbide amounts up to 12 nm (see Table 1).

At $t_{MA} \geq 20$ h the functions $P(H)$, reconstructed from M?ssbauer spectra, exhibit a wide field distribution within the range of 50–300 kOe. It could be connected with the formation of phases based on Fe–C those form Fe_3C after annealing (see Fig. 8, *a*, curves *3*, *5*). The cementite formed exhibits sufficiently wide field distribution as well as a lower (in comparison with the reference data [16]) value of the average field (H = 190 kOe). Most likely, this could be connected with the fact that at a long time of grinding a part of iron atoms in cementite is substituted by titanium forming complex carbide such as $Fe(Ti)_3C$.

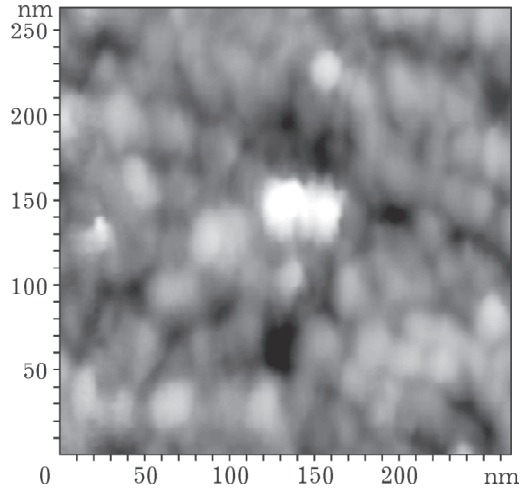

Fig. 9. AFM image for the section of Fe–Ti–toluene sample.

Metallographic studies have revealed no features in the morphology of the particles obtained as the result of MA process in the Fe–Ti mixture in toluene (see Fig. 1, *b*). From AFM data (Fig. 9) one can see that, as opposed to samples Fe–Ti–C and Fe–TiC, the grain structure of particles of Fe–Ti–toluene sample after annealing at 500 °C is homogeneous, with fine grains identical in size.

The scheme of the MA process in this case could be presented as it follows: the formation of nanocrystalline phase, the dissolution of a part of Ti in Fe, thermocatalytic destruction of toluene on fresh-formed metal surface [28], the formation of predominantly TiC owing to a higher enthalpy of its formation (–209 kJ/mol) as compared to the enthalpy of Fe_3C formation (25 kJ/mol) [13]. After the most part of titanium produce TiC, carbon which continues to segregate resulting from the destruction of toluene is bound with Fe to form Fe_3C.

CONCLUSION

1. A sequence of phase structure transformations has been studied for mechanical alloying and annealing of iron– titanium–carbon systems obtained from the mixtures of various compositions: the powders of pure elements such as Fe, Ti and graphite, the powders of Fe and TiC, the powders of Fe, Ti and toluene. In the first case, there is a simultaneous formation of TiC and Fe_3C observed; in the second case, one can observe the dissolution TiC and the formation of secondary TiC and Fe_3C inclusions, whereas in the case of Fe–Ti–toluene sample, first of all TiC, and then Fe_3C are formed.

2. It has been demonstrated that despite of different sequences of phase transformations, in all the cases the final result of MA processing consists in the formation of nanocomposite powders based on the combination of the following phases: solid solution on the basis of Fe, roentgen-amorphous phase on the basis of carbides TiC and Fe_3C, carbide TiC. The relationship between phase components and their morphology depend on the structure of precursors.

3. Annealing results in the decomposition of the amorphous phase and solid solution to produce Fe + TiC + Fe_3C nanocomposite. The dispersity, the amount and the structure of carbide phases formed under annealing the composites depend on the phase structural state of the alloy under investigation after MA procedure. In the case of Fe, Ti and toluene mixture, *via* varying MA duration one could obtain a two-phase system Fe + TiC with the uniform distribution of nanocrystalline phases within the bulk of a sample.

Acknowledgement

Authors express sincere gratitude to D. V. Surnin for performing Auger analysis.

REFERENCES

1 S. S. Kiparisov, Yu. V. Levinskiy, A. P. Petrov, Karbid Titana: Polucheniye, Svoystva, Primeneniye, Metallurgiya, Moscow, 1987.
2 Yu. G. Gurevich, V. K. Narva, N. V. Frage, Karbidostali, Metallurgiya, Moscow, 1988.
3 S. C. Tjong (Ed.), Nanocrystalline Materials: Their Synthesis-Structure-Property Relationships and Applications, Elsevier, Amsterdam, 2006.
4 R. Z. Valiev, I. V. Aleksandrov, Obyomnye Nanostrukturnye Metallicheskiye Materialy, Akademkniga, Moscow, 2007.
5 E. P. Yelsukov, V. V. Ivanov, S. F. Lomaeva, G. N. Konygin, S. F. Zayats, A. S. Kaygorodov, *Perspektivnye Mat.*, 6 (2006) 59.
6 K. Das, T. K. Bandyopadhyay, S. Das, *J. Mat. Sci.*, 37 (2002) 3881.
7 Powder Diffraction File, Alphabetical Index, Inorganic Phases (Int. Center for Diffraction Data, 1601 Park Lane, Swarthmore, Pennsylvania 19081, USA), 1985.
8 E. V. Shelekhov, T. A. Sviridova, *Metallovedeniye i Termicheskaya Obrabotka Metallov*, 8 (2000) 16.
9 E. V. Voronina, N. V. Ershov, A. L. Ageev, Yu. A. Babanov, *Phys. Stat. Sol. (B)*, 160 (1990) 625.
10 T. A. Carlson, Photoelectron and Auger Spectroscopy, Plenum Press, New York, 1975.
11 A. N. Maratkanova, S. F. Lomaeva, I. L. Yakovleva, *Fizika Metallov i Metallovedeniye*, 104, 2 (2007) 184.
12 E. P. Yelsukov, G. A. Dorofeev, A. V. Zagainov, N. F. Vildanova, A. N. Maratkanova, *Mat. Sci. Eng. A*, 369 (2004) 16.
13 V. A. Rabinovich, Z. Ya. Khavin (Eds.), Kratkiy Khimicheskiy Spravochnik, Khimiya, Lenigrad, 1991.
14 El-Eskandarany M. Sherif, *Metallurg. Mat. Trans.*, 27A, 8 (1996) 2374.
15 L. L. Ye, M. X. Quan, *Nanostruct. Mat.*, 5 (1995) 25.
16 T. Massalski (Ed.), Binary Alloys Phase Diagrams, Amer. Soc. Metall., 1987.
17 A. E. Vol, Stroyeniye i Svoystva Dvoynykh Metallicheskikh Sistem, Fizmatgiz, Moscow, 1962.
18 R. A. Arents, Yu. V. Maksimov, I. P. Suzdalev, *Fizika Metallov i Metallovedeniye*, 36, 2 (1973) 277.
19 A. Sh. Bakhtiyarov, V. I. Bobrov, L. N. Vasiliev, *Fizika Metallov i Metallovedeniye*, 47, 6 (1979) 1215.
20 Le G. Caër, P. Matteazzi, *Hyperfine Interact.*, 66 (1991) 309.
21 L. S. Vasiliev, I. L. Lomaev, *Fizika Metallov i Metallovedeniye*, 101, 4 (2006) 417.
22 S. F. Lomaeva, *Deformatsiya i Razrusheniye Materialov*, 3 (2005) 9.
23 L. S. Vasiliev, S. F. Lomaeva, *Kolloid. Zh.*, 65, 5 (2003) 697.
24 E. P. Yelsukov, G. A. Dorofeev, G. A. Fomin, G. N. Konygin, A. V. Zagainov, A. N. Maratkanova, *Fizika Metallov i Metallovedeniye*, 94, 4 (2002) 43.
25 B. S. Bokshtein, Diffuziya v Metallakh, Metallurgiya, Moscow, 1972.
26 E. Gaffet, E. Bernard, J.-C. Niepce, F. Charlot, C. Gras, Le G. Cäer, J.-L. Guichard, P. Delcroix, A. Mocellin, O. Tillement, *J. Mat. Chem.*, 9 (1999) 305.
27 L. S. Vasiliev, E. P. Yelsukov, I. L. Lomaev, *Fizika Metallov i Metallovedeniye*, 102, 2 (2006) 201.
28 S. F. Lomaeva, *Fizika Metallov i Metallovedeniye*, 104, 4 (2007) 403.